RSC Advances

ROYAL SOCIETY OF CHEMISTRY

www.rsc.org/advances

RSC Advances

RSC Publishing

PAPER

Preparation and evaluation of hypocrellin A loaded poly(lactic-co-glycolic acid) nanoparticles for photodynamic therapy

Shan-Shan Qi,[a] Xi Lin,[a] Miao-Miao Zhang,[a] Shu-Zhen Yan, [a] Shu-Qin Yu,†[b] Shuang-Lin Chen*[a]

Abstract: Hypocrellin A (HA), a perylenequinoid pigment isolated from a traditional Chinese medicinal fungus, exhibits excellent antiviral and antitumor property. However, its hydrophobicity, photodegeradation and dark cytotoxity hamper its clinical application. The aim of the present study is to prepare and evaluate a HA loaded poly(lactic-co-glycolic acid) (PLGA) nanoparticles which can be dispersed in water. In this present study, an oil-in-water (O/W) emulsion solvent evaporation technique was employed to fabricate a hypocrellin A loaded poly(D,L-lactic-co-glycolic) nanoparticles. The physiochemical properties and morphological characteristics were examined. The photostability, uptake and *in vitro* phototoxicity and dark toxicity toward A549 cells were evaluated. Scanning electron microscopy (SEM) and confocal laser microscopy (CLSM) images, combined with dynamic light scattering (DLS) measurements and surface charge (ζ-potential) results, showed that the HA-loaded nanoparticles as-prepared were narrowly dispersed with a surface charge of −5.8 mV. The physicochemical properties of the nanoparticles as-prepared were characterized by differential scanning calorimetry (DSC), X-ray powder diffractometry (XRD) and fourier transform infrared (FTIR) spectroscopy. The encapsulation efficiency and drug content were 55.1% and 5.0%, respectively. UV-vis spectra and the results from photobleaching experiments indicated that encapsulation could enhance the photostability of HA. *In vitro* experiments demonstrated that HA loaded PLGA nanoparticles was taken up by A549 cells and exhibited significantly reduced dark cytotoxicity and while maintaining excellent anti-tumor property and ROS production ability. These promising results suggested that nanotechnology provide an intriguing possibility for HA being a potent photosensitizer (PS) in clinical photodynamic therapy (PDT).

1. Introduction

Over the past decades, photodynamic therapy (PDT) has been developed rapidly as an alternative treatment strategy for traditional cancer treatment and gained regulatory approval for the treatment of various diseases, such as cancer and macular degeneration.[1] This is a two-step progress based on photochemical reactions, including accumulation of photosensitizer (PS) and activation by irradiation.[2] After taken up by the cells in a certain time interval, under proper dose and wavelength of irradiation, PS can be activated and thus generate molecular singlet oxygen ($^1O_2$) in the presence of oxygen, which can damage the cells via apoptosis or nercrosis.[3] Considering the PS being a key element in PDT, there are searches for ideal PSs consistently. An ideal PS should have certain properties, such as high singlet oxygen quantum yield, tremendous soluble rate in water without forming aggregates and high absorption in phototherapeutic window.[4]

Hypocrellins, one of the second generations of PSs, have caused increasing attention to its wide absorption band and excellent light-induce singlet oxygen generation ability.[5-7] Hypocrellins was perylenequinoid pigments isolated from the fruiting bodiesof the *Shiraia bambusicola* P. Henn (Fig.1).[8] However, the poor hydrophilicity of hypocrellins highly hampered its clinical applications. Owing to its hydrophobicity, hypocrellins tend to aggregate into clusters in blood and eventually block the vessel.[9] Many efforts have been made to overcome this shortcoming, including different types of nanomedical approaches. A variety of studies mainly focused on encapsulating hydrophobic drugs, including hypocrellins into liposomes to achieve significantly improvement of dispersibility and bioavailability and enhancement of drug efficacy.[10-12] However, developmental work on liposomes has been limited due to inherent problems, such as low encapsulation efficiency and poor storage stability of a liposome suspension. Many attempts also have been made to delivering hypocrellins via silica

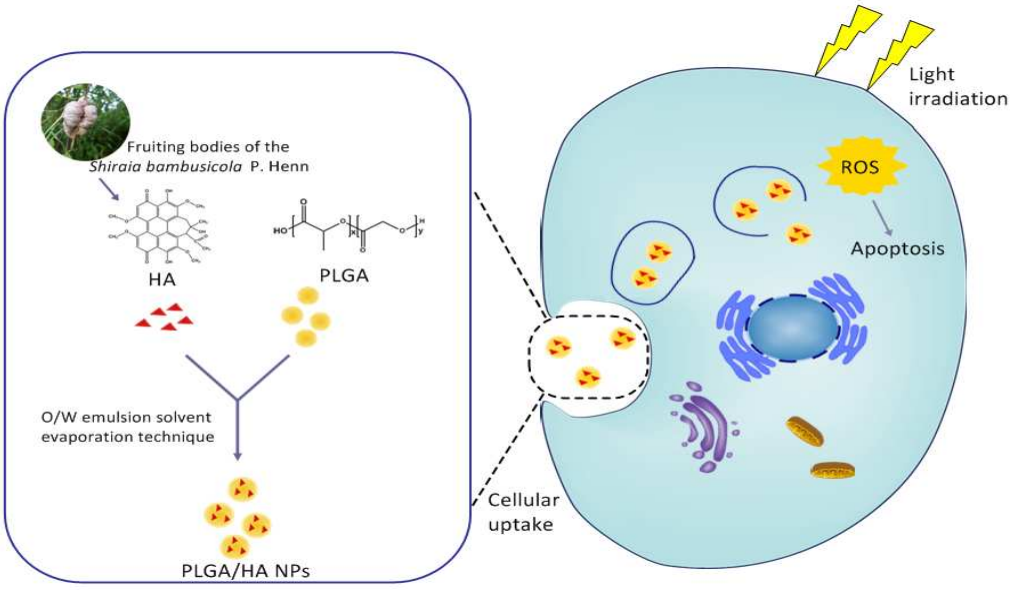

Figure 1 Schematic illustration of preparation of PLGA/HA NPs and its PDT process.

nanoparticles, ignoring the deficiencies of silica in biological metabolism.[13, 14] Moreover, dark toxicity and photodegradation may cause non-specific toxicity in non-targeted cells or organs and counteract the selectivity for PDT.[15] Thus, how to make full use of the characteristic of PLGA to overcome the photodegradation and dark toxicity of hypocrellin subsequently alleviate unwanted side effects is another intriguing challenge.

Recently, various biodegradable delivery systems have been developed for anti-cancer drugs, such as PLGA (Fig.1), hyaluronic acid and saccharide.[16-19] Among these biodegradable materials, PLGA attracted considerable attention. PLGA is one of the commercially available biodegradable approved by the Food and Drug Administration (FDA) for human use.[20] Emerging evidences have shown PLGA nano delivery system also opens new ways for photodynamic therapy, since the nanoparticles encapsulated with PSs have advantages of reduced toxicity, improved dispersibility in plasma, enhanced therapeutic activity and prolonged delivery.[21-24] By now, various PSs have been tested in PLGA nano delivery system for cancer treatment. For instance, 5-aminolevulinic acid (ALA) encapsulated into PLGA gave 65.6 ± 26 nm size particles, an encapsulation efficiency of 65.8% ± 7.2%, and a more effective photo cytotoxicity than free ALA of the same concentration.[25] Another study of *meso-tetra*-(4-hydroxyphenyl) porphyrin (*p*-THPP) yielded a sub-130 nm sized nanoparticles with an increase of intracellular delivery of *p*-THPP.[26] Hence, PLGA uploading HA could be expected to serve as an intriguing delivery system for PDT. However, few reports about PDT for anticancer *in vitro* concerning PLGA nanoparticles loaded with hypocrellin A have been reported yet.

In this work, water-dispersible HA loaded PLGA nanoparticles were prepared for the first time applying the oil-in-water (O/W) emulsion solvent evaporation method and subsequently characterized by SEM, CLSM, DSC, XRD and FTIR. Furthermore, the photostability, cellular uptake, dark toxicity, phototoxicity and ROS level were also explored.

2. Materials and Methods

2.1. Chemicals

Poly(D,L-lactic-co-glycolic acid) (PLGA, L/G = 50/50 , M_W = 30 kDa) was from Jinan Daigang Biomaterial (Shandong, China). Polyvinyl alcohol (PVA, MW = 31 kDa), 2',7'-dichlorofluorescin diacetate (DCFH-DA) and dimethylsulfoxide (DMSO) were obtained from Sigma-Aldrich (MO, USA). Dulbecco's minimum essential medium (DMEM) was from Gibico. Cell Counting Kit-8 (CCK-8) was obtained from Dojindo La boratories (Kumamoto, Japan). Annexin V-FITC Apoptosis Detection kit was obtained from BioVision (USA). Deionized water produced by MilliQ System (Millipore, Paris, France) was utilized throughout the experiments. All other chemicals were of analytical grade.
The irradiation power was a light emitting diode (LED) lamp (90 mW/cm^2; Cidly Optoelectronic Technology Co., Ltd, China) with the wavelength at 470 nm.

2.2. Isolation of HA

HA was isolated from the fruiting bodies (Fig.1) of the *Shiraia bambusicola* P. Henn according to the method reported by Kishi *et al* with slight modification. The air-dried powder of fruit bodies (10.00 g) was extracted with acetone. Organic solvent was evaporated to dryness under vacuum to afford 0.97 g crude extract. After evaporation, the extract was subjected to column chromatography fractionated over silica gel with chloroform-methanol gradient elution. The resulting pigment fraction (260.4 mg) was further separated and purified by preparative thin layer chromatography on silica gel using chloroform-methanol (99:1). Compound 1 (17.3 mg) was subsequently crystallized from acetone. A stock solution of compound 1 at a concentration of 10 mM in DMSO was prepared and stored in the dark at −20 □.

The 1H and 13C NMR data of compound 1 was analyzed by a Bruker Avance Ⅲ 500 spectrometer (Karlsruhe, Germany). MS spectrum was obtained using an Agilent 1290/6460 HPLC/MS/MS spectrometry system with electrospray ionization (ESI) under positive-ion ionization conditions. FTIR spectra were obtained on a

Nexus 670 infrared spectrophotometer (Nicolet, USA) with KBr pellets. UV data were recorded on a Hitachi UV-2450 spectrophotometer using methanol as solvent. Circular Dichroism (CD) measurements were performed on a Chirascan™ CD spectrometer (Applied Photophysics, Leatherhead, UK) using methanol as solvent. XRD data of compound 1 was recorded on a D/max-Rc diffractometer (Ricoh, Japan). DSC measurements were performed on Pyris Diamond calorimeter (Perkin Elmer, USA) at a heating rate of 10 ℃ min^{-1}.

2.3. Preparation of the PLGA NPs or PLGA/HA NPs

PLGA NPs loaded with HA (PLGA/HA NPs) were prepared applying an oil-in-water (O/W) emulsion solvent evaporation technique according to our previous study.[27] Briefly, 10 mg of HA and 100 mg of PLGA were dissolved in acetone (2.5 mL) for 6 h to form a uniform oil phase. The oil phase as-prepared was then injected into 50 mL of a solution PVA (1%, w/v) at about 11,400 rpm under emulsion of a high-speed homogenizer (IKA, Germany). The residual organic solvent was eliminated by mechanically stirring at a constant speed of 1 500 rpm overnight. The NPs were purified by centrifugation (Eppendorf Centrifuge 5418R, Germany) at 13 000 rpm for 30 min at 4 □ and washed twice with distilled water to remove the excess drug and emulsifiers. Finally, the freeze-dried powder of PLGA/HA NPs was obtained after lyophilized for 24 h and stored at 4 □ in the dark before use. Blank NPs were prepared without adding HA in the organic phase employing the same method.

2.4 Characterization of the PLGA/HA NPs

2.4.1 Physicochemical Characterization of the PLGA/HA NPs

After coated with gold for 30 s applying an ion sputtering, the external surface morphology of the HA encapsulated NPs was visualized under a SEM (JSM-5900, JEOL, Tokyo, Japan) at an accelerating voltage of 3 kV.

About 1 mg lyophilized powder of nanoparticles was resuspended in deionized water and sonicated for 10 minutes to fully disperse nanoparticles. The particle size and surface charge were measured under room temperature employing a Malvern Zetasizer 3000 laser diffraction grain size analyzer (Worcesterhire, UK).

Thermal analysis was determined using a DSC (Pyris Diamond, Perkin Elmer, USA). Each sample (PLGA, HA, and PLGA/HA NPs) in sealed standard aluminum pans was heated at a rate of 10 □ min^{-1} from 25 to 270 □ under dry nitrogen atmosphere.

XRD measurements of PLGA, HA, and PLGA/HA NPs were observed employing a D/max-Rc diffractometer (Ricoh, Japan) with Cu K radiation at a voltage of 40 kV and 200 mA. The scanning rate was 2 min^{-1} over the interval 3 to 40°.

FTIR spectra of each sample (PLGA, HA, and PLGA/HA NPs) was determined applying the method as described above.

2.4.2. Drug Encapsulation Efficiency and Drug Loading Content

The amount of HA encapsulated in PLGA/HA/NPs as-prepared was investigated by UV absorbance at 464 nm. A standard curve was established using standard solutions of HA in methanol from 0 to 24 μg mL^{-1}. Accurately weighed quantity of lyophilized NPs was dissolved in 10 mL of methanol completely to extract HA. Then, the samples were sonicated for 10 min to leach out entire HA. After centrifuged at 13 000 rpm for 30 min, the absorbance of supernatant at 464 nm was measured. The amount of entrapped drug was calculated based on the calibration curve. The measurements were repeated in triplicate. Blank NPs were used as controls.

Drug loading content (LC) and drug encapsulation efficiency (EE) were calculated according to the following equations, respectively:

$$drug\ loading\ content\ (\%) = \frac{weight\ of\ HA\ in\ nanopartic les}{weight\ of\ nanopartic les} \times 100 \quad (1)$$

$$encapsulat ion\ efficiency\ (\%) = \frac{weight\ of\ HA\ in\ nanopartic les}{weight\ of\ total\ HA} \times 100 \quad (2)$$

2.4.3 *In Vitro* Release Studies

The release kinetics of HA loaded NPs were performed by the dialysis method. PLGA/HA NPs (5 mg) were suspended in 1 mL distilled water and sealed in a dialysis membrane bag (cutoff MW 12 kDa, Millipore, France). The dialysis bags containing nanoparticles were immersed in 100 mL PBS (pH 7.4 and 6.5) with 0.5% (w/v) Tween-80 in a conical flask, respectively, followed by a constant shaking at a speed of 100 rpm at 37 □. At appointed time, a volume of 3 mL release medium was withdrawn, followed by immediately adding the same volume of fresh buffer solution. The released HA was measured by UV-vis spectrophotometer as mentioned above. All assays were carried out in triplicate.

The drug release rate (RR) was calculated according to the following formula:

$$drug\ \ release\ \ rate\ = \frac{HA\ \ released\ \ amount}{total\ \ amount\ \ of\ \ HA\ \ in\ \ NPs} \times 100 \quad (3)$$

2.4.4 Photophysical Characterization and Photostability Study

Photophysical character and photostability of HA loaded NPs were investigated by UV-vis spectrophotometer. PLGA/HA NPs were dispersed in phosphate buffered saline (PBS; pH 7.4) to yield a uniform dispersion. HA was dissolved in PBS with same pH with the aid of methanol (0.5%). The as-prepared solution was sonicated for about 15 min and centrifuge at 13,000 rpm for 30 min to obtain the saturated PBS solution of HA. According to Diwu's method, PBS solutions of PLGA/HA NPs was adjusted to give approximate optical density before photobleaching assay.[5] All these samples were illuminated in a standard 1 cm path length quartz cuvette by a high pressure mercury lamp (500 W) and its UV-vis data in the visible region were recorded by a Shimadzu UV-2450 spectrophotometer (Japan).

Photobleaching experiments were conducted to compare the photostability of HA before and after encapsulation. After the initial absorbance values was recorded by a UV-vis spectrophotometer, PBS solution of HA or dispersion of PLGA/HA NPs was exposed to the irradiation of a LED-lamp with the wave length of 470 nm. At designated time points, 5 mL of each sample was taken out and was examined at the wavelength of 464 nm. The measurements were repeated in triplicate.

The photostability of HA was calculating according as follows:

$$photobleaching\ percentage\ of\ HA\ (\%) = \frac{C_o - C_t}{C_o} \times 100 \quad (4)$$

In the above equation, C_0 represents the concentration of HA before irradiation, and C_t represents the concentration of HA at t h.

2.5 Cell Culture

A549 human lung adenocarcinoma cells line was purchased from American Type Culture Collection (ATCC, USA). A549 cells were cultured in Dulbecco's Modified Eagle's Medium (DMEM) supplemented with 10% (v/v) fetal bovine serum (FBS) 100 IU mL^{-1} penicillin, and 100 μg mL^{-1} streptomycin at 37 □ in a humidified incubator gassed with 5% CO_2.

2.6 Photodynamic Activity Assay and Dark Cytotoxicity Assays

The A549 cells were seeded onto 96-well plates at density of 2×10^4 cells per cm^2 and incubated at 37 □. After 24 hours, cells were washed with PBS and was incubated a series of concentrations of HA or PLGA/HA NPs at equivalent HA concentration from 0.5 to 2.5 μM. DMSO (0.1%, v/v) was used as co-solvent. The cells without any treatment were used as controls. The cells incubated with culture medium containing 0.1% DMSO were used as DMSO controls. After 24 h incubation in the dark, the cells were washed three times with PBS and irradiated by a light emitting diode (LED) lamp with the wavelength at a power peak 470 nm for 15 min. After irradiation, the cells were incubated in the dark at 37 □ for 18 h before survival assessment. Cell viability was estimated using Cell Counting Kit 8 according to the protocol outlined by manufacturer. Finally, the absorbance intensity was measured at a wavelength of 450 nm. Following the same protocols, PDT treatments were also performed with cells treated with blank PLGA NPs at doses equivalent to the tested HA loaded NPs, to exclude any toxic effect brought by the nano drug carrier alone.

The cell viability and cell viability ratio was determined using following formula:

$$cell\ \ viability\ \ (\%) = \frac{OD_{treated}}{OD_{control}} \times 100 \qquad (5)$$

$$cell\ viability\ ratio = \frac{cell\ viability\ before\ irradiation}{cell\ viability\ after\ irradiation} \qquad (6)$$

where $OD_{treated}$ is the absorbance intensity of the cells incubated with the HA or NP suspension and $OD_{control}$ is the absorbance intensity of the cells incubated with the culture medium only.

For dark cytotoxicity studies, cells were treated follow exactly the same procedure as cell viability was mentioned in photodynamic activity assay, except for the light treatment.

2.7 Measurement of Reactive Oxygen Species （ROS）

The generation of intracellular peroxides was determined by applying the probe 2',7'-dichlorofluorescin diacetate (DCFH-DA). Briefly, approximately 2×10^4 per cm^2 cells was seeded in fluorescence 96-well microplate and incubated overnight for attachment. After washed with PBS, cells was incubated a series of concentrations of HA or NPs at equivalent HA concentration from 0.5 to 2.5 μM for 4 h. The DMSO control and the empty nanoparticles group as mentioned above were also introduced. The cells treated with H_2O_2 (20 μM) were used as positive controls. For the light group, then PDT treatment was conducted as described above. After incubated for 30 min, the cells were washed and incubated with 10 μM of DCFH-DA for 20 min at room temperature without light. Then the cells were washed twice with PBS to remove the excess probe. Finally, the fluorescence intensity was detected with the excitation and emission wavelengths of 500 and 485nm, respectively.

The ROS level and ROS production ratio was determined using following formula:

$$ROS\ level\ \ (Fold) = \frac{fluorescence\ intensity\ of\ \ treated\ \ group}{fluorescence\ \ intensity\ of\ \ control\ group} \qquad (7)$$

$$ROS\ \ production\ ratio = \frac{ROS\ \ producted\ \ after\ irradiation}{ROS\ \ producted\ before\ irradiation} \qquad (8)$$

where the treated group is the cells incubated with the HA or NP suspension and the control group is the cells incubated with the culture medium only.

For the dark group, cells were treated follow exactly the same procedure as light group, except for the light treatment.

2.8 Nanoparticle Uptake

To determine the cellular uptake of the nanoparticles, we seeded onto the cover glasses at 1×10^5 cells per cm^2 in the 6-well. The cells were washed and incubated with PLGA/HA NPs with equivalent concentration of HA at 2.5 μM for 4 h after attachment. After incubated with nanoparticles, the A549 cells were gently washed three times with PBS. After the cells were washed with PBS, the cellular uptake and time-dependent intracellular accumulation of NPs was visualized under laser scanning confocal microscope (Flowview FV1000, Olympus, Japan).

2.9 Measurement of Aberrant Exposure of Phosphatidylserine Residues

For investigation of the apoptosis induced by HA or HA loaded NPs, A549 cells were incubated with HA or PLGA/HA NPs (with the equivalent concentration of HA at 2.5 μM) in the dark. After 4 h incubation, unbound drugs were washed away by PBS. For the light group, the cells were exposed to irradiation of LED-light for 15 min. The dark group was incubated without irradiation. The cells without any treatment were used as controls. After light treatment, the cells of two groups were incubated for the rest 18 h at 37 □. Cells were harvested and 1×10^6 cells were washed and resuspended with PBS. Eventually, after Annexin V-FITC (fluoresceine isothiocyanate) staining, apoptosis induced by HA or PLGA/HA/NPs were evaluated immediately using flow cytometry. Each sample was analyzed utilizing a flow cytometry FACSVantage system (Becton Dickinson, California, USA). Cells that bound Annexin V-FITC were analyzed using 488 nm for excitation and 530 nm for emission.

2.10 Statistical Analysis

A software package SPSS 17.0 (SPSS Inc., Chicago, USA) was applied for statistical analysis. All results were expressed as mean ± standard deviation (SD). Student t-test was used for comparisons of the means. P values less than 0.05 was considered statistically significant.

3. Results and discussion

3.1. Identification of HA

The extraction ratio of compound 1 is 1.73 mg/g. Compound 1: dark red crystals, mp 216.4 ℃ (Supporting Information). UV λ_{max}(MeOH)/nm 267, 341, 464, 540 and 580 nm (Fig. 2A); IR ν_{max}/cm^{-1} 3469 (OH), 1700 (CO) and 1608 (aromatic ring) (Fig. 2B); NMR δ_H(500 MHz, $CDCl_3$) 15.96 (1H, s, -OH···O-), 15.92 (1H, s, -OH···O-), 6.57 (1H, s, 8-CH=), 6.55 (1H, s, 5-CH=), 4.11 (3H × 2, s, -OMe × 2), 4.07(3 H × 2, s, -OMe × 2), 3.515 (1H, d, J_{AB} = 12.0 Hz, 13-CH_A), 2.635 (1H, d, J_{AB} = 12 Hz, 13-CH_B), 3.45 (1H, s, 15-CH), 1.89 (1H, s,18-Me), 1.71 (1H, s, 16-Me) and 1.63 (1H, br. s, 14-OH); δ_C(500 MHz, $CDCl_3$) 27.0, 30.1, 41.9, 56.5, 56.6, 60.8, 61.7, 62.1, 78.8, 102.0, 102.1, 106.7, 106.9, 117.7, 118.2, 125.0, 127.6, 128.5, 133.2, 134.0, 150.6, 150.9, 167.5, 170.9, 171.8, 179.8, 180.3 and 207.4 (Supporting Information); ESI-MS m/z 547 ($[M+H]^+$) calcd for $C_{30}H_{26}O_{10}$ on the basis of MS data (Fig. 2C), ^{1}H- and ^{13}C-NMR spectra.

Furthermore, the absolute configuration of compound 1 was also confirmed by comparing CD spectrum with previous study (Fig. 2D). Compound 1 and isocercosporin (P(S)) have the same axial chirality.

Compound 1 was determined to be hypocrellin A after comparing the ^{1}H-, ^{13}C-NMR data, MS, DSC, FTIR,UV and CD spectrum with those of hypocrellins in literature.[8]

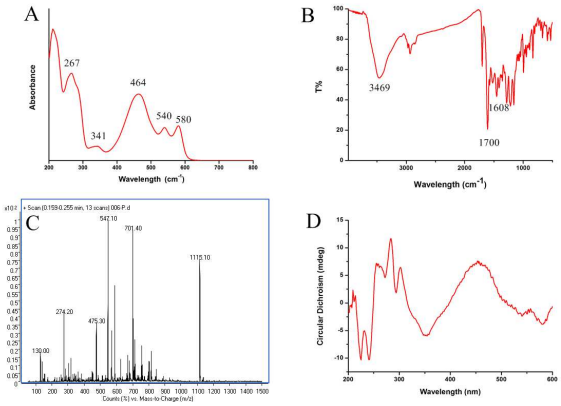

Figure 2 Characterization of HA. (**A**) UV-vis spectra, (**B**) FTIR spectra, (**C**) ESI-MS spectra and (**D**) CD spectra of HA.

3.2 Preparation and Physicochemical Characterization of Nanoparticles

Various approaches have been proposed to formulate PLGA NPs by dispersing the preformed polymers, among which emulsion solvent evaporation (O/W) technique was chosen to fabricate polymeric NPs in this work.[28] Polyvinyl alcohol (PVA) is applied as the emulsifying agent during the process, because the nanoparticulate carrier formulated employing this emulsifier are comparatively homogeneous, small-size and redispersible in aqueous solution.[29, 30]

SEM image of HA loaded NPs was present in Fig. 3, suggesting the NPs has a distribution over the range of about 20−200 nm with spherical shape. Inset panel of Fig. 3 was in consistent with the particle size in SEM. The ζ potential of HA loaded NPs and blank NPs was -5.8 and -7.3 mV, respectively, which might attributed to the dissociation of the carboxylic end groups of PLGA (Table 1).

In previous studies, surface charge and size of the nanoparticles play a critical role concerning cellular uptake.[31, 32] On the one hand, a potential advantage of nano-scale particle size is that it could contribute to increase residence time in blood and improve biodistribution of the carrier via EPR effect, which subsequently bring a passive selective tumor targeting and delivery.[33] On the other hand, as cationic particles can bind more efficiently to most cells surface before reaching the target location, it might be crucial to maintain the nano-size carriers either anionic or neutral for less untargeted binding and thereby reduce unexpected side effect.[32]

DSC was employed to find out the crystal transformation of the nanoparticles. As demonstrated in Fig. 4A, the melting peak of crystalline HA appeared at 216.4 □, consistent with published literature.[8] PLGA polymer gives rise to a small peak around 45 □, corresponding to its glass transition temperature. However, no notable peak was found from the curves of the HA loaded NPs except the same glass transition temperature at around 45 □, indicating that HA conversed from crystalline form to amorphous from.

X-ray diffraction (XRD) measurements was carried out to observe the interactions between HA and PLGA. The Fig. 4(B) clearly showed the characteristic peak of HA appeared at 8.020°,14.180°, 16.100°, 25.380° and 26.680°, indicating the crystalline structure of HA. However, these characteristic peaks disappeared in the curve of NPs, which suggested the HA was no longer existed as crystalline form and successfully entrapped into the NPs.

Table 1 Drug encapsulation efficiency (EE), drug loading content (LC) and zeta potential (ZP) determination for nanoparticles

	EE (%)	LC (wt.%)	ζ (mV)
Blank NPs	-	-	-7.3
PLGA/HA NPs	55.1 ± 1.05	5.0 ± 0.10	-5.8

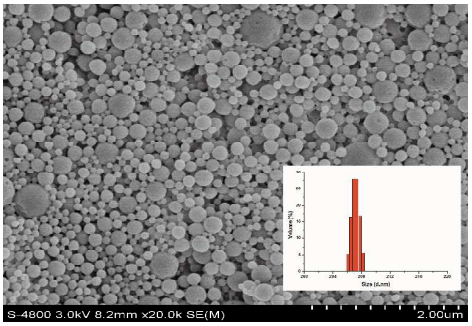

Figure 3 Morphology property and size distribution of PLGA/HA NPs.

To learn more about the physicochemical characteristic of PLGA/HA NPs, FTIR was carried out. The FTIR spectra of HA, PLGA and PLGA/HA NPs was shown in Fig. 4(C) and (D). The characteristic band of PLGA at 1685 cm^{-1} and 3413 cm^{-1} corresponded to the C=O group and O-H group, respectively. For the spectra of HA, the sharp peak at 1608 cm^{-1} would be ascribed to the characteristic band of the aromatic ring of HA. The characteristic peak of HA at 1700 cm^{-1} was attributed to the C=O stretching vibration, which was slightly shifted to 1760 cm^{-1} in the spectrum of the NPs. This could be attributed to the formation of intermolecular hydrogen bonds between C=O group of PLGA and the O−H group of HA.

From the results presented above, we can come to a conclusion that, PLGA/HA/NPs were successfully formulated and negatively charged with spherical shaped and a narrow size distribution. Meanwhile, the SEM and CLSM study proved that the PLGA/HA NPs was nano-scale, which could improve the water dispersibility and biocompatibility.

3.3 Drug Loading Content and Encapsulation Efficiency

To study the drug encapsulation efficiency (EE) and drug loading content (LC) of PLGA/HA NPs, the UV-vis spectrophotometer method was introduced. The absorbance values at 464 nm were found to be linearly correlated with HA concentrations ranging from 0 to 24 μg mL^{-1} with a correlation coefficient of 0.999. As shown in Table 1, the drug loading content and encapsulation efficiency of the PLGA/HA NPs were 5.0% and 55.1%, respectively.

3.4 *In Vitro* Release of HA from PLGA/HA NPs

The *in vitro* release study of HA from HA loaded NPs over a seven-day period was present in Fig. 5. PH 7.4 and 6.5 PBS were selected as the release phase, simulating physiological environment and tumor extracellular environment.[34] As depicted in Fig. 5, in both cases, the drug release kinetics displayed a biphase release with a fast release in the first 24 hours and a slower release during the rest of test time. In the first 24 hours, 28.2% and 27.4% of HA was released from at pH 7.4, 6.5, respectively. By the end of the test

time, a maximum of 49.6% of HA released from NPs was achieved at pH 6.5, which were much faster than that at pH 7.4 (38%).

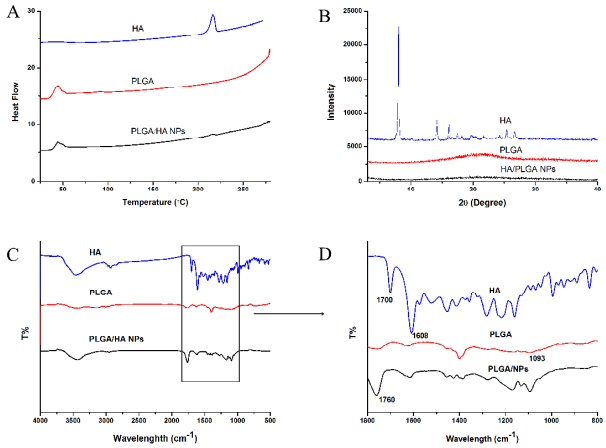

Figure 4 Physicochemical characterization of HA, PLGA and PLGA/HA NPs. (A) DSC curves, (B) XRD patterns, and (C), (D) FTIR spectra of HA, PLGA and PLGA/HA NPs.

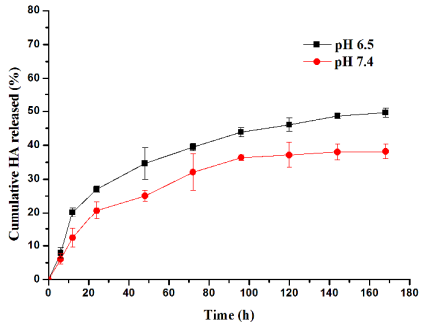

Figure 5 *In vitro* cumulative release of HA from the PLGA/HA NPs.

The fast release rate of HA at the beginning stage could be attributed to the release of HA from the external surface of PLGA/HA NPs. The entrapped HA in the PLGA substrate of nanocarriers is released at a significantly slower rate, which is mainly due to diffusion of the polymeric substrate, thus giving a nano-formulation of sustained release with remarkable photodynamic effects.[35] Another noticeable phenomenon is that the release rate of HA from the nanoparticles at pH 6.5 was higher than in artificial blood physiological environment (pH 7.4), indicating that the PLGA/HA NPs were stable at the blood circulation with less non-specific release. On the other hand, this characteristic might encourages HA to release more in tumor area via passive targeting. It is widely believed that tumor tissue has some unique anatomical and pathophysiological characteristics of vasculature, like high vascular density and ineffective lymphatic system, which bring "enhanced permeability and retention" (EPR) effect. Maeda and his group first managed to design NPs to achieve tumor targeting delivery taking advantage of EPR effect.[36] The enhanced accumulation of NPs, combined with its release kinetic and good water-dispersibility, could contribute to a favorable biodistribution of HA and more selective targeting of HA loaded nanoparticles to tumors.

3.5 Photophysical Characterization and Photostability Study

Freezed-dried HA loaded PLGA NPs was found to dispersible in water, while free HA can hardly dissolve in water matrix without the help of other solvents (Fig. 6A). To investigate the absorption spectrum of HA and PLGA/HA NPs, UV-vis spectrophotometer was applied. As shown in inset panel in Fig. 6B, free HA in PBS (pH 7.4) has three characteristic absorbance bands, found at 465 nm, 534 nm and 586 nm, respectively. After encapsulated into PLGA, the characteristic absorbance band at 464 nm was red-shifted slightly to 473 nm. The UV spectra suggested that HA preserved its photoactivity after nanoencapsulation.

In order to observe the photostability of HA and PLGA/HA NPs, photobleaching experiment was introduced. After the PBS dispersion of HA loaded PLGA NPs or solution of HA were irradiated by a LED-lamp with a wavelength at 470 nm, the intensity of the absorption peaks decreased with the irradiation time (Fig. 6B). At the last time point, photobleaching efficiencies of HA loaded NPs and free HA are 18.34% and 38.64%, respectively, indicating that HA encapsulated into PLGA own improved photostability than free HA because of the protection of the PLGA.

Most PSs, including HA, are not photostable. In simple medium along with in complex dispersion or solution, photo-induced bleaching of PSs reduces their fluorescence intensity and initial absorption, which consequently lower its photosensitive effect. According to our study, photobleaching experiments of HA and PLGA/HA NPs dispersions indicated that the absorption intensity of HA decreased notably in water, which is in consistent with Zhou's study.[13] For this phenomenon, the probable reason is either non-radiative decay promotedby drug-solvent interaction or concentration quench processes come from self-aggregation of HA. But after encapsulated into PLGA, the inside HA molecules (non-polar drug) can be protected against the exposure to polar medium, such as aqueous solution. The protection effect provided by PLGA nanoparticles offers enhanced photostability of HA against

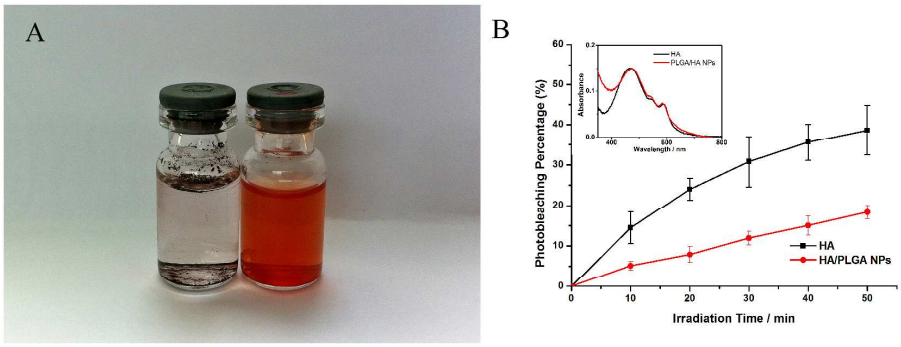

Figure 6 Dispersibility, photophysical characterization and photostability study. (A) Photo images of HA and PLGA/HA NPs in water. (B) Photobleaching experiments of HA and PLGA/HA NPs (inset picture: absorption spectra of HA and PLGA/HA NPs in pH 7.4 buffer).

photobleaching.

3.6 Cell Viability and ROS Detection

The *in vitro* dark cytotoxicity and photodynamic activity of free HA and PLGA/HA NPs was shown in Fig. 7A and B, respectively. Without irradiation, a sharp decrease of cell viability was observed with the HA concentration from 0.5 μM to 2.5 μM (Fig. 7A). On the other hand, the PLGA/HA NPs were nearly non-toxic at all tested concentrations when incubated with cells in the dark, whereas at concentrations above 2 μM, the cytotoxicity delivered by free HA was much higher.

Unlike the dark cytotoxicity, when LED light was applied, the situation became different. Both the free HA and the NPs were highly toxic to A549 cells with slightly decreasing tendency with the increase of concentrations when exposed to LED-light, even at the minimum concentration of 0.5 μM the cell viability was still 20.8% and 23.4% (Fig. 7B).

Since the first time DCFH-DA was applied in hydrogen peroxide detection assay, it became popular to use it as a indicator to evaluate intracellular reactive oxygen species formation.[37] The nonpolar probe DCFH-DA crosses cell membranes and is enzymatically hydrolyzed to nonfluorescent dichlorofluorescin (DCFH). In the presence of reactive species, nonfluorescent DCFH would be oxidized to dichlorofluorescein (DCF) which emits strong fluorescence. The ROS detection data was shown in figure 8. Without irradiation, the level of ROS in HA treated group was significantly higher than PLGA/HA NPs treated group at the concentration of 2.5 μM. When being exposed to LED light, HA treated group at five tested concentrations produced slightly more ROS than PLGA/HA NPs, which is basically consistent with cell toxicity results.

Both data or results of cell viability ratio (Fig. 7C) and ROS production ratio (Fig. 8C) suggested that nano-formulation of HA had better toxicity selectivity toward A549 cells at relatively high concentration.

Cellular uptake of HA or HA loaded PLGA NPs was visualized using a laser scanning confocal microscope in A549 cells (Fig. 9). The fluorescence of HA excited by the 543 nm laser makes it readily detectable by CLSM after cellular uptake. The CLSM images showed that PLGA/HA NPs emitting red fluorescence was mainly accumulated in the cytoplasm. Furthermore, the nano-formulated HA was internalized more actively than free HA, which is presumably through an endocytic process, according to former studies conducted by Panyam *et al*.[38]

Fei *et al* proved that in the absence of illumination HA could still directly result in the death of HeLa cells, which brings the potential risks of its dark toxicity.[39] Once the NPs were internalized by endocytosis, PLGA/HA NPs were in the endosomal compartments and released HA from PLGA in a sustained way. The release kinetics, combined with cellular uptake mechanism of PLGA/HA NPs, may help to alleviate the negative effect of hypocrellin A in the non-targeted area, eventually lead to a lower dark toxicity. When the light was applied, the activated HA released from nanoparticles might eventually kill A549 cells. However, further evaluation is needed to find out it possible cell death mechanism.

3.8. Analysis of Apoptosis

Since Dougherty and his college first demonstrated PDT can be harnessed to kill tumor cells in 1978, varieties of the PSs have been investigated *in vitro* or *in vivo* to understand the mode of cell death.[40] According to latest studies, the mechanism of cell death by PDT may be either apoptosis or necrosis, which is largely depending on the photochemistry and photophysics property of the PSs.[2, 41] Recently, increasing number of studies suggested that hypocrellin is a strong inducer of cell apoptosis. Moreover, reactive oxygen species (ROS) generated by PS in the presence of irradiation and oxygen might play a pivotal role in this apoptosis process, especially singlet oxygen.[42] From the above evidence, PLGA/HA NPs might induce the cell death via a similar mechanism.

To further confirm our speculation, the apoptosis assay was carried out. Phosphatidylserine externalization is one of critical

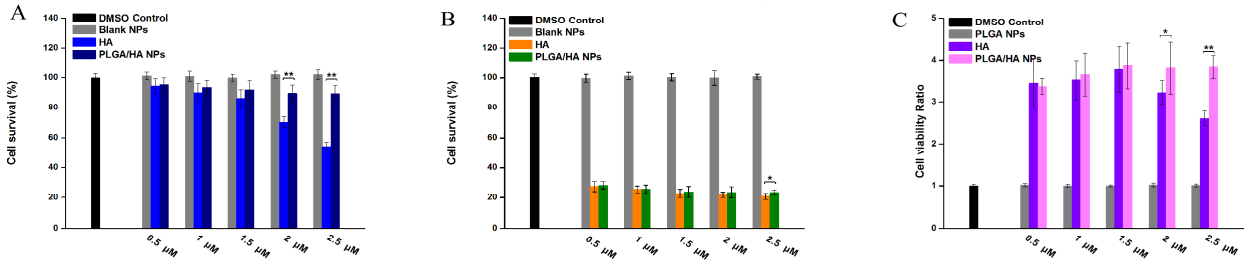

Figure 7 Dark cytoxicity assays (A) and photodynamic activity assays (B) on A549 cells. *p < 0.05; **p < 0.01 (t-test).

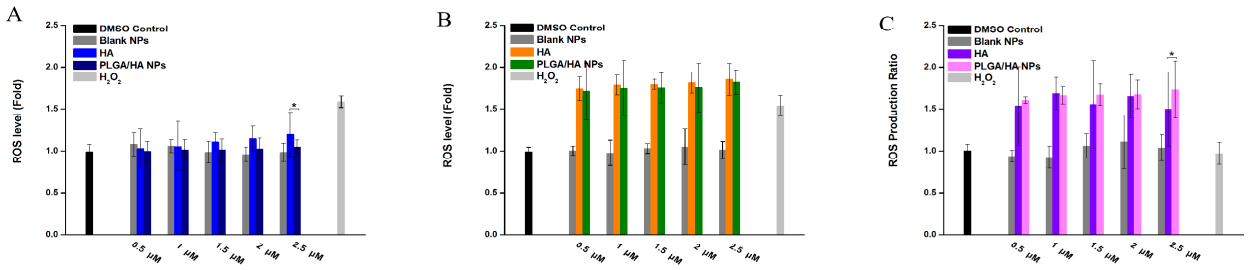

Figure 8 ROS level before PDT (A), after PDT (B) and ROS production ratio (C) on A549 cells. *p < 0.05; **p < 0.01 (t-test).

3.7. Cellular Uptake Assays

events related to incidence of apoptotic death in tumor cells in response to various kinds of stimuli, such as PS. Phosphatidylserine

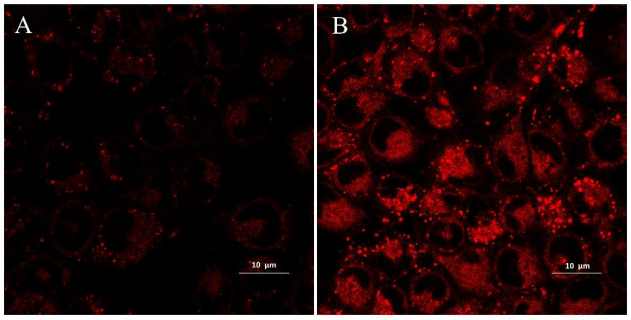

Figure 9 Confocal laser microscopy images of A549 cells incubated with HA (A) and PLGA/HA/NPs (B) with equivalent HA concentration (2.5 μM) (magnification 100×).

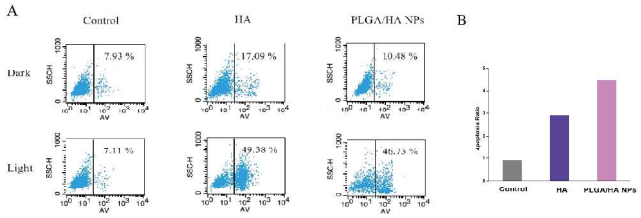

Figure 10 Phosphatidylserine externalization assays on A549 cells (A) and the apoptosis ratio with or without irradiation (B).

exposure at the exterior surface of A549 cells was evaluated using flow cytometry with the FITC-labeled annexin V staining following the manufacturer's instructions. The concentration of 2.5 μM was chosen because of its better toxicity selectivity. After activated by LED-light both HA and PLGA/HA NPs increased expression of phosphatidylserine on interior surface of cell membrane (49.38% and 46.73%), indicating loss of phospholipd asymmetry (Fig. 10). However, without irradiation, the phosphatidylserine externalization of cells incubated with HA was evidently more than the cells incubated with PLGA/HA NPs with equivalent concentration of HA, confirming a much stronger cellular destruction of free HA.

4. Conclusions

In summary, a novel water-dispersible HA loaded PLGA NPs have been fabricated applying oil-in-water (O/W) emulsion solvent evaporation technique based on the superior character of PLGA, which is biodegradable and biocompatible. The HA loaded PLGA nanoparticles were narrowly distributed with spherical shape and negative surface charge. The result HA-loaded PLGA nanoparticles have enhanced photostability and can be actively internalized by A549 cells. The notable decrease of dark cytotoxicity was observed, which is likely due to negative surface charge and preferably drug release of nanoparticles at lower pH. Based on the above results, it can be concluded that the PLGA nano drug delivery system could provide a promising future for HA in the field of anticancer PDT.

Acknowledgements

This study was supported by National Key Technology Research and Development Program of the Ministry of Science and Technology of China (Project No. 2012BAD36B0502).

Notes and references

[a] College of Life Sciences, Nanjing Normal University, Nanjing 210023, The People's Republic of China, Tel/Fax: +86 25 8589 1571; E-mail: chenshuanglin@njnu.edu.cn

[b] Jiangsu Key Laboratory for Supramolecular Medicinal Materials and Applications, College of Life Sciences, Nanjing Normal University, Nanjing 210023, The People's Republic of China,Tel/Fax: +86 25 8589 1265; E-mail: yushuqin@njnu.edu.cn

† This author is the second corresponding author.

1. M. Triesscheijn, P. Baas, J. H. M. Schellens, F. A. Stewart, *Oncologist*, 2006, **11**, 1034-1044.
2. C. A. Robertson, D. H. Evans, H. Abrahamse, *J Photochem Photobiol B*, 2009, **96**, 1-8.
3. N. L. Oleinick, R. L. Morris, I. Belichenko, *Photoch Photobio Sci*, 2002, **1**, 1-21.
4. E. Paszko, C. Ehrhardt, M. O. Senge, D. P. Kelleher, J. V. Reynolds, *Photodiagn Photodyn Ther*, 2011, **8**, 14-29.
5. Z. Diwu, C. Zhang, J. W. Lown, *Anticancer Drug Des*, 1993, **8**, 129-143.
6. Z. Diwu, *Photochem Photobiol*, 1995, **61**, 529-539.
7. Z. Zhiyi, W. Nenghui, W. Qian, L. Meifan, *Free Radic Biol Med*, 1993, **14**, 1-9.
8. T. Kishi, S. Tahara, N. Taniguchi, M. Tsuda, C. Tanaka, S. Takahashi, *Planta Med*, 1991, **57**, 376-379.
9. F. Wang, L. Zhou, J. H. Zhou, X. T. Gu, Y. Y. Feng, *J Therm Anal Calorim*, 2010, **102**, 69-74.
10. D. Bai, X. Xia, C. M. Yow, E. S. Chu, C. Xu, *Eur J Pharmacol*, 2011, **650**, 496-500.
11. C. Yu, S. Chen, M. Zhang, T. Shen, *Photochem Photobiol*, 2001, **73**, 482-488.
12. Y. Liu, J. Fang, Y. J. Kim, M. K. Wong, P. Wang, *Mol Pharm*, 2014, **11**, 1651-1661.
13. L. Zhou, Y. W. Ning, S. H. Wei, Y. Y. Feng, J. H. Zhou, B. Y. Yu, J. Shen, *J Mater Sci-Mater M*, 2010, **21**, 2095-2101.
14. Z. B. Li, J. G. Wang, J. R. Chen, W. H. Lei, X. S. Wang, B. W. Zhang, *Sci China Chem*, 2010, **53**, 1994-1999.
15. A. Master, M. Livingston, A. Sen Gupta, *Journal of Controlled Release*, 2013, **168**, 88-102.
16. B. Sivakumar, R. G. Aswathy, Y. Nagaoka, S. Iwai, K. Venugopal, K. Kato, Y. Yoshida, T. Maekawa, D. N. Sakthi Kumar, *Rsc Adv*, 2013, **3**, 20579.
17. S. K. Tripathi, S. Gupta, K. C. Gupta, P. Kumar, *Rsc Adv*, 2013, **3**, 15687.
18. Z. Yu, R. M. Schmaltz, T. C. Bozeman, R. Paul, M. J. Rishel, K. S. Tsosie, S. M. Hecht, *J. Am. Chem. Soc.*, 2013, **135**, 2883-2886.
19. C. Bhattacharya, Z. Yu, M. J. Rishel, S. M. Hecht, *Biochemistry*, 2014, **53**, 3264-3266.
20. F. Danhier, E. Ansorena, J. M. Silva, R. Coco, A. Le Breton, V. Préat, *J Control Release*, 2012, **161**, 505-522.
21. M. Zeisser-Labouèbe, N. Lange, R. Gurny, F. Delie, *Int J Pharm*, 2006, **326**, 174-181.
22. A. J. Gomes, A. S. Faustino, A. E. Machado, M. E. Zaniquelli, T. de Paula Rigoletto, C. N. Lunardi, L. O. Lunardi, *Drug Deliv*, 2006, **13**, 447-454.
23. C. L. da Silva, J. O. Del Ciampo, F. C. Rossetti, M. V. Bentley, M. B. Pierre, *Photochem Photobiol*, 2013, **89**, 1176-1184.
24. A. Vargas, N. Lange, T. Arvinte, R. Cerny, R. Gurny, F. Delie, *J Drug Target*, 2009, **17**, 599-609.
25. L. Shi, X. Wang, F. Zhao, H. Luan, Q. Tu, Z. Huang, H. Wang, H. Wang, *Int. J. Nanomedicine*, 2013, 2669.

26. Y. N. Konan, J. Chevallier, R. Gurny, E. Allemann, *Photochem Photobiol*, 2003, **77**, 638-644.
27. X. Xie, Q. Tao, Y. Zou, F. Zhang, M. Guo, Y. Wang, H. Wang, Q. Zhou, S. Yu, *J. Agric. Food Chem.*, 2011, **59**, 9280-9289.
28. C. E. Astete, S. C. M., *J. Biomater. Sci. Polymer Edn*, 2006, **17**, 247-289.
29. S. K. Sahoo, J. Panyam, S. Prabha, V. Labhasetwar, *J Control Release* 2002, **82** 105-114.
30. C. Wischke, Y. Zhang, S. Mittal, S. P. Schwendeman, *Pharm Res*, 2010, **27**, 2063-2074.
31. C. He, Y. Hu, L. Yin, C. Tang, C. Yin, *Biomaterials*, 2010, **31**, 3657-3666.
32. K. Y. Win, S. S. Feng, *Biomaterials*, 2005, **26**, 2713-2722.
33. S. Acharya, S. K. Sahoo, *Adv. Drug Delivery Rev.*, 2011, **63**, 170-183.
34. J. Wang, J. Sun, Q. Chen, Y. Gao, L. Li, H. Li, D. Leng, Y. Wang, Y. Sun, Y. Jing, S. Wang, Z. He, *Biomaterials*, 2012, **33**, 6877-6888.
35. T. Niwa, H. Takeuchi, T. Hino, N. Kunou, Y. Kawashima, *J Control Release*, 1993, **25**, 89-98.
36. M. S. Cartiera, K. M. Johnson, V. Rajendran, M. J. Caplan, W. M. Saltzman, *Biomaterials*, 2009, **30**, 2790-2798.
37. A. S. Keston, R. Brandt, *Anal. Biochem.*, 1965, **11**, 1-5.
38. J. Panyam, W. Z. Zhou, S. Prabha, S. K. Sahoo, V. Labhasetwar, *FASEB J*, 2002, **16**, 1217-1226.
39. X. F. Fei, J. Chen, K. Y. Zheng, W. Wei, S. J. Sun, L. Wang, L. Ma, C. Li, L. R. Teng, *Chem Res Chinese U*, 2006, **22**, 772-775.
40. T. J. Dougherty, J. E. Kaufman, A. Goldfarb, K. R. Weishaupt, D. Boyle, A. Mittleman, *Cancer Res*, 1978, **38**, 2628-2635.
41. D. Lihuan, Z. Jingcun, J. Ning, W. Guozeng, C. Yiwei, L. Wei, Q. Jing, Z. Yuanfang, C. Gang, *Lasers Surg Med*, 2014, **46**, 319-334.
42. Y.-H. Kim, *Oncol. Rep.*, 2013.